The EMBO Journal (2009) 28, 3602–3612 | © 2009 European Molecular Biology Organization | All Rights Reserved 0261-4189/09
www.embojournal.org

THE EMBO JOURNAL

Mg^{2+}-dependent gating of bacterial MgtE channel underlies Mg^{2+} homeostasis

Motoyuki Hattori[1,6], Norihiko Iwase[2,6], Noritaka Furuya[2,6], Yoshiki Tanaka[1], Tomoya Tsukazaki[1], Ryuichiro Ishitani[1], Michael E Maguire[3], Koichi Ito[1,4,*], Andres Maturana[5,*] and Osamu Nureki[1,2,*]

[1]Department of Basic Medical Sciences, Institute of Medical Science, The University of Tokyo, Minato-ku, Tokyo, Japan, [2]Department of Biological Information, Graduate School of Bioscience and Biotechnology, Tokyo Institute of Technology, Midori-ku, Yokohama-shi, Kanagawa, Japan, [3]Department of Pharmacology, Case Western Reserve University, Cleveland, OH, USA, [4]Precursory Research for Embryonic Science and Technology (PRESTO), Japan Science and Technology Agency (JST), Minato-ku, Tokyo, Japan and [5]Global Edge Institute, Tokyo Institute of Technology, E31, Tokyo, Japan

The MgtE family of Mg^{2+} transporters is ubiquitously distributed in all phylogenetic domains. Recent crystal structures of the full-length MgtE and of its cytosolic domain in the presence and absence of Mg^{2+} suggested a Mg^{2+}-homeostasis mechanism, in which the MgtE cytosolic domain acts as a 'Mg^{2+} sensor' to regulate the gating of the ion-conducting pore in response to the intracellular Mg^{2+} concentration. However, complementary functional analyses to confirm the proposed model have been lacking. Moreover, the limited resolution of the full-length structure precluded an unambiguous characterization of these regulatory divalent-cation-binding sites. Here, we showed that MgtE is a highly Mg^{2+}-selective channel gated by Mg^{2+} and elucidated the Mg^{2+}-dependent gating mechanism of MgtE, using X-ray crystallographic, genetic, biochemical, and electrophysiological analyses. These structural and functional results have clarified the control of Mg^{2+} homeostasis through cooperative Mg^{2+} binding to the MgtE cytosolic domain.

The EMBO Journal (2009) **28,** 3602–3612. doi:10.1038/emboj.2009.288; Published online 1 October 2009
Subject Categories: membranes & transport; structural biology
Keywords: electrophysiology; gating mechanism; ion channel; structural biology

*Corresponding authors. O Nureki or A Maturana or K Ito, Department of Basic Medical Sciences, Institute of Medical Science, The University of Tokyo, 4-6-1 Shirokanedai, Minato-ku, Tokyo 108-8639, Japan.
Tel.: +81 3 6409 2125; Fax: +81 3 6409 2127;
E-mail: nureki@ims.u-tokyo.ac.jp or Tel.: +81 258 47 9445;
Fax: +81 47 258 9400; E-mail: maturana@vos.nagaokaut.ac.jp or
Tel.: +81 3 5449 5309; Fax: +81 3 5449 5415;
E-mail: itopi005@ims.u-tokyo.ac.jp
[6]These authors contributed equally to this work

Received: 26 March 2009; accepted: 4 September 2009; published online: 1 October 2009

Introduction

Magnesium ion is an essential metal element for life and has a crucial function in many biological process, such as ATP utilization, activation of and catalysis by hundreds of enzymes, and maintenance of genomic stability (Hartwig, 2001; Cowan, 2002). In human beings, abnormal Mg^{2+} homeostasis is reportedly associated with several diseases, including cardiovascular disease, diabetes, and high blood pressure (Alexander *et al*, 2008). However, among the major biological cations, the mechanisms of Mg^{2+} transport and homeostasis are only slowly being elucidated. Recently, three groups reported the crystal structures of the CorA Mg^{2+} transporter, which provided the first structural framework of a Mg^{2+} transporter (Nelson and Kennedy, 1971; Hmiel *et al*, 1986; Eshaghi *et al*, 2006; Lunin *et al*, 2006; Payandeh and Pai, 2006).

The MgtE family of Mg^{2+} transporters is ubiquitously distributed in all kingdoms of life (Moomaw and Maguire, 2008). In *Bacillus subtilis*, the gene expression of MgtE is primarily regulated by a Mg^{2+}-sensing riboswitch (M-box riboswitch) in response to intracellular Mg^{2+} levels, and probably also in other Gram-positive bacteria, which would contribute to relatively long-term Mg^{2+} homeostasis (Dann *et al*, 2007). In mammals, SLC41 transporters, which are distant MgtE homologues, were found to function in Mg^{2+} homeostasis (Goytain and Quamme, 2005a, b; Sahni *et al*, 2007; Kolisek *et al*, 2008). In bacteria, MgtE consists of the N-terminal cytosolic domain and the C-terminal transmembrane domain. On the other hand, the SLC41 transporters lack the cytosolic domain. Despite its apparently significant function in Mg^{2+} homeostasis, the Mg^{2+}-transport mechanism of MgtE is poorly understood, and it is not even clear whether MgtE functions as either a channel or an active transporter.

Recently, we reported the crystal structures of the full-length MgtE of *Thermus thermophilus* at 3.5 Å resolution and of its cytosolic domain in the presence and absence of Mg^{2+} at 2.3 and 3.9 Å resolutions, respectively (Hattori *et al*, 2007a). The full-length structure of MgtE in the presence of Mg^{2+} revealed a homodimer. The putative ion-conducting pore in the TM domain is closed in this crystal form through interactions between the TM domains and the 'plug helices' connecting the cytosolic and TM domains. Several putative Mg^{2+} ions are bound to the interface between the dimeric cytosolic domains or between the cytosolic and TM domains. A structural comparison of the cytosolic domains in the presence and absence of Mg^{2+} revealed a drastic Mg^{2+}-dependent structural transition involving the rotation of the plug helices. On the basis of these structures, we proposed a Mg^{2+}-homeostasis mechanism in which the cytosolic domain of MgtE acts as a 'Mg^{2+} sensor' to regulate the gating of the ion-conducting pore through plug helix movement by sensing the intracellular Mg^{2+} concentration. Molecular dynamics simulations of the MgtE cytosolic domain also suggested that its multiple

Mg^{2+}-binding sites induce the conformational transition in a cooperative manner (Ishitani *et al*, 2008). The model comprehensively provided a short-period intracellular homeostasis mechanism for acute environmental changes. However, there has been no complementary functional analysis to substantiate the gating mechanism or even to determine whether MgtE is gated by the intracellular Mg^{2+} concentration. Moreover, the limited resolution of the full-length structure prevented the unambiguous identification of these divalent-cation-binding sites.

Here, we established the channel properties and the Mg^{2+}-dependent gating of MgtE by a combination of X-ray crystallographic, genetic, biochemical, and electrophysiological analyses to address the functional mechanism of the Mg^{2+} regulation of MgtE. Our data indicated that MgtE functions as a Mg^{2+}-dependent gating channel and that the cooperative Mg^{2+} binding to the cytosolic domain stabilizes the closed conformation of the channel. On the basis of these results, we have proposed a novel structural transition mechanism of MgtE.

Results

MgtE structure with divalent-cation-binding sites

In the earlier full-length MgtE structure, several putative Mg^{2+} ions apparently bind to the cytosolic domains, which would induce the stabilization of the closed conformation of MgtE. However, the limited resolution (3.5 Å) of the full-length structure did not allow an unambiguous identification of these divalent-cation-binding sites. To test the Mg^{2+}-dependent gating model, the precise divalent-cation-binding sites of MgtE should be clarified. Therefore, we determined a higher resolution structure of the full-length MgtE. By extensive screening of detergents for MgtE crystallization, we obtained a new crystal form of MgtE in the presence of Mg^{2+}, which diffracts to a higher resolution (2.94 Å) than the earlier crystal form (3.5 Å). The updated structure of the full-length MgtE is shown in Figure 1. The overall structure of the new crystal form is quite similar to that of the earlier-reported MgtE, with an RMSD value of 0.9 Å for all of the Cα atoms, and represents the closed conformation. On the other hand, some parts of the electron density of the updated structure have been improved. As a result, we found significant differences between the current and earlier structures.

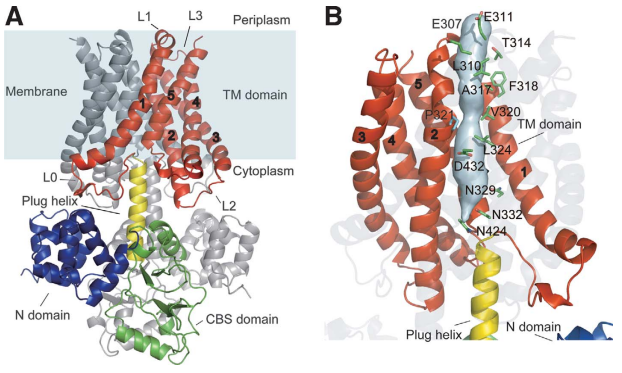

Figure 1 The 2.9-Å resolution MgtE structure. (**A**) The MgtE dimer is viewed in the membrane plane, with the N domain (blue), the CBS domain (green), the plug helix (yellow), and the transmembrane (TM) domain (red) highlighted in one subunit. The other subunit is coloured grey. The TM helices of one subunit are numbered. The membrane surface is indicated. (**B**) Solvent-accessible surface of the ion-conducting pore. Residues lining the pore are indicated.

First, in the earlier structure, the electron density around Pro321, lining the putative ion-conducting pore, was ambiguous, and the preceding portion of the TM2 helix apparently adopted a non-helical, flexible structure (Hattori *et al*, 2007a). On the other hand, in the current structure, this region is restructured to extend the TM2 helix, which is kinked at Pro321 (Figure 1B). It is noteworthy that the region around Pro321 is the narrowest part of the pore, which would prevent ion conduction in the closed state. In addition, the hydrophobic residues near the periplasmic side would also prevent the ion conduction (Figure 1B). These regions at the periplasmic side of MgtE may create a strong barrier to ion permeation. Therefore, in addition to the interaction between the plug helices and the TM domains on the cytosolic side of MgtE (Hattori *et al*, 2007a), the MgtE pore would be closed on both the periplasimic and cytosolic sides. Moreover, for MgtE to adopt an open conformation, the TM2 helices of both subunits should move apart at the position of Pro321, in addition to the movement of the plug helices. Such a putative 'hydrophobic gate' has also been observed in the closed-state structure of the CorA Mg^{2+} channel (Lunin *et al*, 2006), the inwards rectifying potassium channel (Kuo *et al*, 2003) and the nicotinic acetylcholine receptor (Miyazawa *et al*, 2003). Interestingly, although these other channels use bulky hydrophobic residues to form the gates, MgtE seems to use small hydrophobic residues with a kinked main chain structure.

Second, in the new crystal form, an additional strong electron density peak was observed between the conserved acidic residues Glu59 in the N domain of one monomer and Asp226 in the CBS domain from the other subunit (Figure 2D; Supplementary Figure S1). We interpreted the electron density as an additional Mg^{2+} ion (Mg7), based on the same criteria as earlier used to assign the other putative-bound Mg^{2+} ions (Figure 2A–D) (Hattori *et al*, 2007a).

Certain divalent cations, such as Co^{2+} or Ni^{2+}, bind to Mg^{2+}-binding sites by mimicking the octahedral coordination geometry of Mg^{2+} (Eshaghi *et al*, 2006). To confirm that the earlier-assigned bound Mg^{2+} were indeed Mg^{2+}, this new crystal form was used for soaking experiments with Co^{2+} and Ni^{2+}, to distinguish the divalent-cation-binding sites by the anomalous signals derived from these heavier cations. The anomalous difference Fourier maps of the Co^{2+}-soaked crystals clearly supported our assignment of all of the cytosolic Mg^{2+}-binding sites (for Mg2–7) (Figure 2F and G). The data from the Ni^{2+}-soaked crystal provided results exactly consistent with those from the Co^{2+}-soaked crystal (Supplementary Figure S2). In contrast to the Mg2–7-binding sites in the cytosolic domain, the Mg1-binding site in the TM domain could not be confirmed with either the Co^{2+} or Ni^{2+} anomalous signal (Figure 2E; Supplementary Figure S2A). This result indicates that Co^{2+} and Ni^{2+} ions might not be able to access the Mg1-binding site at the centre of the pore in the crystalline state, because of the current closed structure. This is consistent with the idea that the ion-conducting pore is closed on both the periplasmic and cytosolic sides in the closed state of MgtE. Altogether, we could confirm 12 Mg^{2+} (Mg2–7 for two monomers)-binding sites in the cytosolic domain of MgtE.

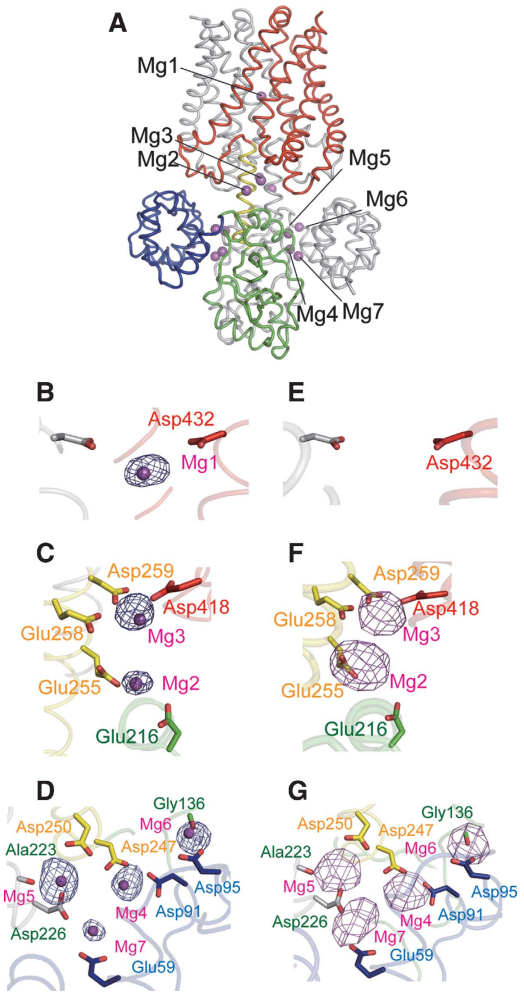

Figure 2 Divalent-cation-binding sites. (**A**) Side view of the overall structure with the bound Mg^{2+}. (**B**–**D**) Close-up view of the respective Mg^{2+} (Mg1–7)-binding sites, with an F_o-F_c omit map contoured at 4.0 σ, calculated with the full-length structure excluding Mg^{2+}. (**E**–**G**) Anomalous difference Fourier map derived from Co^{2+}-soaked crystals, contoured at 5.0 σ, at the Mg1–7-binding sites.

MgtE acts as a highly selective Mg^{2+} channel

To functionally verify our structure-based mechanism of ion conduction and Mg^{2+}-dependent gating by MgtE, we have developed two types of analyses to evaluate its Mg^{2+}-transport activity: *in vivo* complementation and *in vitro* patch-clamp analyses. Although a *Salmonella* strain lacking two major Mg^{2+}-transporter genes, *mgtA* and *corA*, reportedly exhibits Mg^{2+} auxotrophy and has been used for *in vivo* functional analyses of Mg^{2+} transporters (Kehres and Maguire, 2002), *Escherichia coli* K12 strains with the same gene knockouts unexpectedly did not show Mg^{2+} auxotrophy (data not shown). This fact, unfortunately, prevented researchers from adopting the many useful analytical tools established in *E. coli* genetics. By a systematic search for additional component(s) involved in major Mg^{2+} transport in the *mgtA* and *corA* knocked-out *E. coli* background, the novel gene *yhiD*, encoding an integral membrane protein related to MgtC, was successfully assigned as the candidate of the third component. We generated a Mg^{2+}-auxotrophic *E. coli* K12 strain, devoid of the major set of genes for Mg^{2+} transport, *corA*, *mgtA*, and *yhiD*, which can survive only when supplemented with a sufficiently high concentration (100 mM) of Mg^{2+}. The result newly indicated that the yhiD gene would be an essential component for the Mg^{2+} uptake system in *E. coli*. When we transformed the strain with the full-length wild type (WT) MgtE gene, the cells could survive in Mg^{2+}-free LB medium, whereas the control empty vector could not complement the Mg^{2+} auxotroph (Figure 3A), suggesting that the exogenously expressed WT MgtE is clearly capable of reconstituting Mg^{2+}-transport activity *in vivo*. The expression of the MgtE proteins in the membrane fraction was confirmed by anti-His tag western blotting (Supplementary Figure S3).

Then, we generated giant spheroplasts (Martinac *et al*, 1987; Kuo *et al*, 2007) of the same transformants of the Mg^{2+}-auxotrophic *E. coli* strain for the patch-clamp experiments (Supplementary Figure S4). Our newly generated Mg^{2+}-auxotrophic *E. coli* strain has the advantage of expressing the genes encoded in the pET vector under the control of the strong T7 promotor, which enables us to overexpress MgtE in the generated giant spheroplasts. Thus, the giant spheroplasts transformed with the *mgtE*-pET plasmid could be efficiently used for a patch-clamp analysis, because of the high expression of the MgtE channel. Using a Mg^{2+}-sensitive dye, mag-fluo4, we confirmed that MgtE is functionally expressed in the giant spheroplasts. Mg^{2+} influx is readily apparent in giant spheroplasts expressing MgtE under 10 mM sucrose condition as well as under 300 mM sucrose, but not in those carrying the control empty vector (Supplementary Figure S5).

We measured the MgtE-associated currents in the patch-clamp analysis by excising membrane patches from the MgtE-expressing giant spheroplasts. Currents were recorded at test potentials ranging from −70 to +30 mV. The pipette solution (corresponding to the extracellular region, $[Mg^{2+}]_{out}$) included 90 mM $MgCl_2$, whereas the bath solution (corresponding to the intracellular region, $[Mg^{2+}]_{in}$) contained 0.2 mM $MgCl_2$. The results clearly showed representative currents reflecting the open and closed states of a single MgtE channel (Figure 3B). In contrast, cells carrying the control empty vector did not show this activity (Figure 3B). The current was strictly dependent on the presence of Mg^{2+} in the pipette, and its amplitude increased with increasingly negative membrane potentials (Figure 3C), which is consistent with Mg^{2+} permeation through the expressed MgtE channel. The current–voltage relationship determined at negative membrane potential yielded a slope conductance of 96 ± 2.7 pS (Figure 3C) at −40 mV, corresponding to a transport efficiency of $\sim 3 \times 10^7$ ions/s at −60 mV, which is much higher that those of active transporters. The current did not depend on the bath pH (Supplementary Figure S6). These results strongly favour a channel-type mechanism for MgtE.

To further characterize the single channel properties of MgtE, we examined the ion-conduction selectivity for other divalent cations (Co^{2+}, Ni^{2+}, Mn^{2+}, and Ca^{2+}) (Figure 3D and E). The pipette solution and the bath solution included 90 and 0.2 mM divalent cations, respectively. Currents were apparently observed for Co^{2+}, but not for Ni^{2+}, Mn^{2+}, and Ca^{2+} (Figure 3D and E), whereas cells carrying the control empty vector did not show activity with any of these cations (data not shown). The current–voltage relationship determined at negative membrane potential yielded a conductance

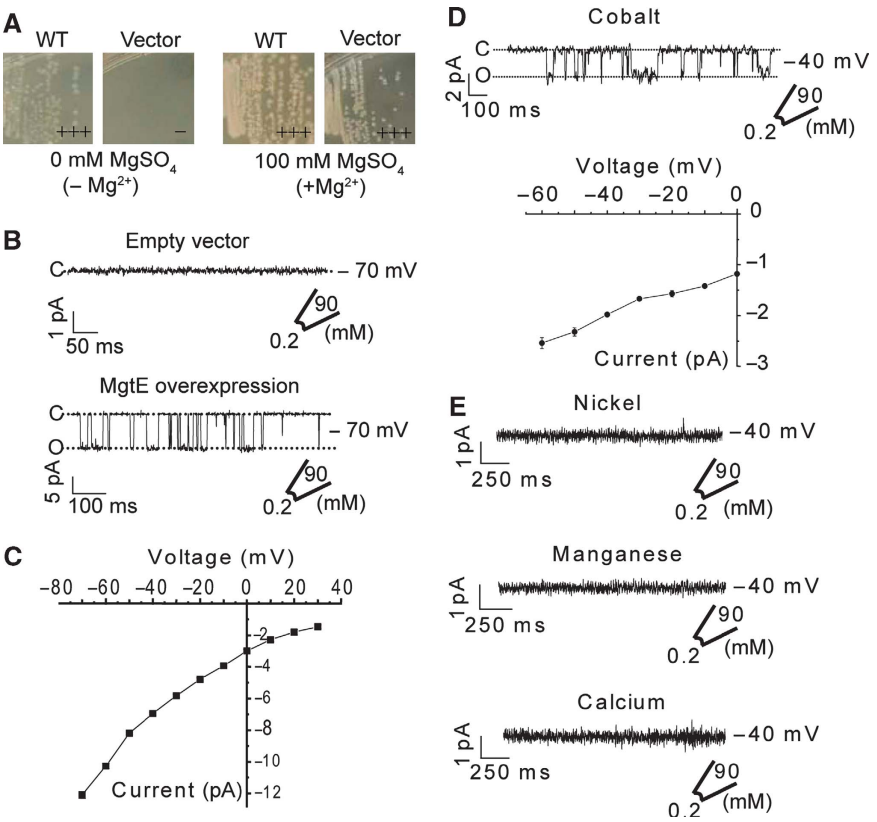

Figure 3 Mg^{2+} channel activity of MgtE. (**A**) Growth complementation of the Mg^{2+}-auxotrophic strains harbouring either WT or empty vector in the presence ($+Mg^{2+}$, 100 mM $MgSO_4$) or absence ($-Mg^{2+}$, 0 mM $MgSO_4$) of supplementary Mg^{2+}. Growth of each transformant is indicated as '+++' (similar to that of empty vector in the presence of 100 mM $MgSO_4$), '++' (less), '+' (much less), '+/–' (severe growth retardation), and '–' (no growth at all). (**B**) Single channel currents were measured in the inside–out configuration from *E. coli* spheroplasts. An example of current traces recorded from control (upper) and MgtE-overexpressing triple knock-out *E. coli* spheroplasts (bottom) at −70 mV. (**C**) The current–voltage relationship between −70 and +40 mV was determined from the single current amplitude at the indicated potentials. Values are mean and standard error of the mean (s.e.m.) of 10 experiments. (**D**) The Co^{2+} permeability of the MgtE channel was determined by measuring the current in the presence of 90 mM $CoCl_2$. The current–voltage relationship was determined by the single current amplitude. (**E**) The permeabilities of nickel, manganese, and calcium were also tested. Traces are examples of currents recorded at −40 mV. Each experiment was performed four times.

of 22 ± 1.6 pS with 90 mM Co^{2+}, which is much smaller than that with Mg^{2+}. The low but considerable level of Co^{2+}-transport activity, which coincides with the earlier studies on MgtE (Smith *et al*, 1995), suggests that MgtE might also be involved in the uptake of Co^{2+} as a micronutrient. On the other hand, Co(III) hexammine, an analogue of fully hydrated Mg^{2+} and a well-characterized inhibitor of the CorA Mg^{2+} channel (Kucharski *et al*, 2000; Kolisek *et al*, 2003; Schindl *et al*, 2007), completely blocked Mg^{2+} influx through MgtE (Supplementary Figure S7). This inhibition by Co(III) hexammine suggests that a fully hydrated Mg^{2+} ion initially binds to MgtE. Altogether, these results clearly show that MgtE functions as a highly selective Mg^{2+} channel.

Ion-conducting pore in the MgtE structure

To identify the ion-conducting pathway of the MgtE channel, we designed structure-based mutants of MgtE. To evaluate their ability to transport Mg^{2+}, we used a growth-complementation system using the Mg^{2+}-auxotrophic *E. coli* strain.

The MgtE homodimer seems to be stabilized by electrostatic interactions between the monomers within the low-dielectric environment of the membrane. Mutations of the highly conserved polar residues involved in these dimer interactions (R285A, Q333A, and E359A) (Figure 4A; Supplementary Figure S1) abolished the Mg^{2+}-transport activity, as shown by the complementation assay (Figure 4B). These results support our hypothesis that stable homodimer formation is requisite for ion conduction.

We then mutated the conserved residues that line the putative ion-conducting pore. Mutations of the hydrophobic residues near the periplasmic side (F318A, P321A, L324A in Figure 1B) eliminated the growth-complementation activity (Figure 4C). Furthermore, mutations of the conserved hydrophilic residues at the centre of the pore (N329A, D432A, and D432N in Figure 1B; Supplementary Figure S1) also abolished the complementation activity (Figure 4C). Thus, Asp432, which binds Mg1, is proposed to be an ion-selective site of MgtE. The patch-clamp analyses of the D432A and N329A mutants revealed that they also lost transport activity *in vitro* (Figure 4D), supporting the proposal that this site is crucial for Mg^{2+} transport. The expression and integration of all of the MgtE mutants in the membrane fraction was confirmed by anti-His tag western blotting (Supplementary Figure S3). Furthermore, the gel filtration analysis of the purified D432A mutant showed a similar elution profile to that of the purified WT MgtE, regardless of the presence of Mg^{2+}

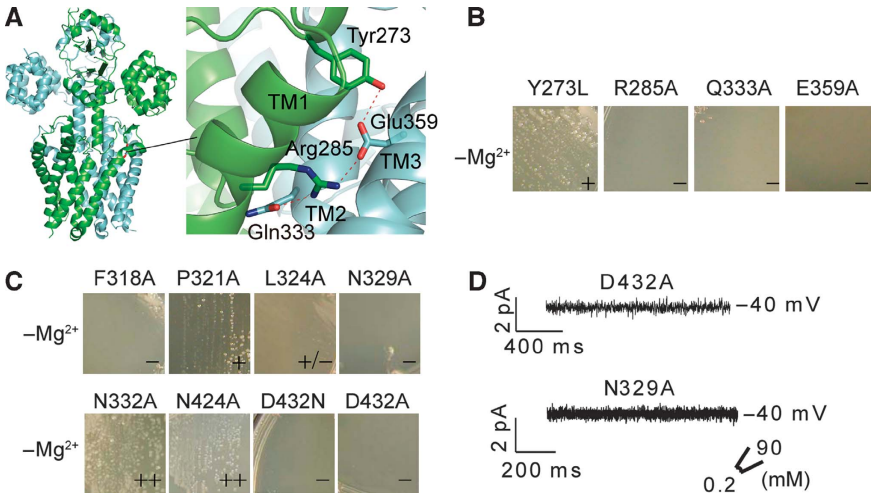

Figure 4 Ion-conducting pore of MgtE. (**A**) TM domain residues involved in molecular dimerization. Hydrogen and ionic bonds are shown as dotted lines. The backbones of the two subunits are coloured green and blue, respectively. (**B**) Mg^{2+}-auxotrophic growth complementation by mutated MgtE (Y273L, R285A, Q333A and E359A) genes on the $-Mg^{2+}$ plates. (**C**) Mg^{2+}-auxotrophic growth complementation by mutated MgtE (F318A, P321A, L324A, N329A, N332A, N424A, D432N, and D432A) genes on the $-Mg^{2+}$ plates. (**D**) Mutations of the conserved hydrophilic residues in the pore inhibit the MgtE current. Examples of currents recorded at −40 mV from membrane patches of spheroplasts overexpressing the D432A and N329A mutants. The pipette solution and the bath solution included 90 and 0.2 mM $MgCl_2$, respectively. Each experiment was repeated four times.

(Supplementary Figure S8). The result implies that the D432A mutant, which lost the putative Mg^{2+}-binding site in the TM domain and the transport activity, would retain the channel assembly ability. On the other hand, it is well established that the permeant ions of potassium channels have a very important function in the stabilization of the channel assembly (Splitt *et al*, 2000).

Mutations of the polar residues at the cytosolic end (N332A and N424A in Figure 1B) had either a slight or no effect on the ability to rescue the Mg^{2+}-auxotrophic growth (Figure 4C). These results are reasonable, as these residues are replaced with alanine in the MgtE channels from other organisms (Supplementary Figure S1). In the open-form structure, this part of the pore would be exposed to the cytosolic vestibule, suggesting that it might not be crucial for ion permeation. In addition, these *in vivo* complementation results were further supported by an *in vivo* transport assay of $^{57}Co^{2+}$ (Supplementary Figure S9). In summary, these results support the proposal that the MgtE pore, formed by the dimerized TM domain, functions as the 'ion-conducting pore'.

Gating control of MgtE by the intracellular Mg^{2+} concentration

On the basis of our earlier structures, we proposed that MgtE is involved in cytosolic Mg^{2+} homeostasis by an ability to sense the intracellular Mg^{2+} concentration through the cytosolic Mg^{2+}-binding sites (Hattori *et al*, 2007a). To verify this hypothesis, we examined the effect of $[Mg^{2+}]_{in}$ on the MgtE channel activity (Figure 5). As the $[Mg^{2+}]_{in}$ in the bath solution was increased from 0.2 to 10 mM, the current progressively decreased (Figure 5A–D). The addition of Mg^{2+} to the bath will change the driving force for Mg^{2+}. This means that the equilibrium potential will be shifted to a more positive voltage, thus reducing the current. It can be estimated that the reduction of the current because of the change in driving force should be about 17% for $[Mg^{2+}]_{in} = 1$ mM, as compared with $[Mg^{2+}]_{in} = 0.2$ mM, 25% for $[Mg^{2+}]_{in} = 5$ mM, and 42% for $[Mg^{2+}]_{in} = 10$ mM at −40 mV with a conductance of 96 pS. This means that currents of about 5.8 pA for $[Mg^{2+}]_{in} = 1$ mM, about 5.3 pA for $[Mg^{2+}]_{in} = 5$ mM, and about 4 pA for $[Mg^{2+}]_{in} = 10$ mM should be measured at −40 mV, considering that a current of around 7 pA was measured at −40 mV in 0.2 mM $MgCl_2$. For $[Mg^{2+}]_{in} = 1$ and 5 mM, the measured amplitudes are consistent with those of the predicted amplitudes (Figure 5E). In contrast, for $[Mg^{2+}]_{in} = 10$ mM, we could not measure any current (Figure 5D), which means that the channel is completely closed at least at 10 mM intracellular Mg^{2+} concentration. Quantitatively, an increase in $[Mg^{2+}]_{in}$ drastically reduced the open probability (Figure 5F). Thus, the MgtE channel was completely inactivated between 5 and 10 mM $[Mg^{2+}]_{in}$ (Figure 5C–F). The threshold for MgtE inactivation by $[Mg^{2+}]_{in}$ is approximately consistent with the results from the earlier Mg^{2+}-dependent protease protection analysis of MgtE (Ishitani *et al*, 2008). Altogether, these results indicate that the intracellular Mg^{2+} concentration is capable of regulating the MgtE channel activity.

If the intracellular Mg^{2+} ions regulate the MgtE activity, then the MgtE cytosolic domain must be able to discriminate Mg^{2+} from other divalent cations. Therefore, to further explore the ion-sensing mechanism by the MgtE cytosolic domain, we examined whether the Mg^{2+}-transport activity is affected by the near-cognate Ca^{2+} (Figure 5G and H; Supplementary Figure S10). The presence of 20 mM $[Ca^{2+}]_{in}$ completely inactivated the Mg^{2+}-transport activity (Figure 5H). In contrast, 0.2 mM $[Ca^{2+}]_{in}$ had no effect on the activity (Figure 5G and Supplementary Figure S10). Moreover, the threshold for MgtE inactivation by $[Ca^{2+}]_{in}$ resides in the millimolar range, which is also consistent with the earlier-reported protease protection of MgtE by Ca^{2+} (Ishitani *et al*, 2008). Nonetheless, as the intracellular Ca^{2+}

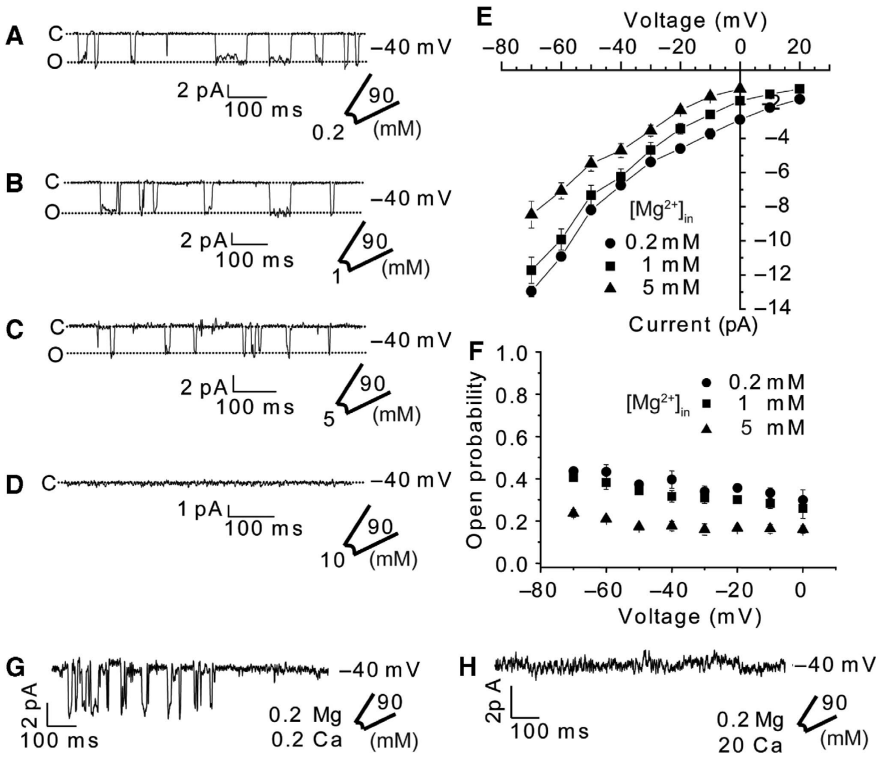

Figure 5 Mg^{2+} dependence of the MgtE channel activity. (**A**–**D**) The $MgCl_2$ concentration in the bath was increased from 0.2 to 1 mM and 5 to 10 mM, and single currents were measured at each $MgCl_2$ concentration with MgtE-overexpressing spheroplasts. Example of current traces recorded at −40 mV from a single membrane patch at different $[Mg^{2+}]_{in}$. (**E**) The current–voltage relationships of the MgtE current recorded at different $[Mg^{2+}]_{in}$ were determined with a single current amplitude. (**F**) The open probability was determined at the different $[Mg^{2+}]_{in}$ ($n = 5$ for each condition), without plotting the data for the 10-mM $MgCl_2$ conditions, because there was no opening of the channel under these conditions. (**G**, **H**) Example of current recorded at −40 mV from membrane patches of WT MgtE-overexpressing spheroplasts with low and high concentrations of $CaCl_2$. The bath solution was exchanged from 0.2 to 20 mM $CaCl_2$, and the currents were recorded at each $CaCl_2$ concentration. Traces are representative of the current recorded at −40 mV in four spheroplasts.

concentration (under physiological conditions) is in the micromolar range (Outten and O'Halloran, 2001), Ca^{2+} is unlikely to exert any physiologically relevant effect. This situation is also applicable to other divalent cations, as their intracellular concentrations are usually lower than that of Ca^{2+} (Outten and O'Halloran, 2001). On the other hand, based on the molecular dynamics simulation of the cytosolic domain of MgtE, Na^+ binding to the cytosolic domain did not induce the structural transition to the closed form (Ishitani *et al*, 2008). Therefore, the MgtE cytosolic domain might not seem to sense monovalent cations, such as Na^+ ion. To test this hypothesis, we performed the limited proteolysis and the patch-clamp analysis under conditions with a high concentration of monovalent cation (Na^+ or K^+) (Supplementary Figure S11). The protease protection assay revealed that MgtE was highly susceptible to proteolysis at low-intracellular concentrations (0–100 mM), but was not at high-intracellular concentrations (200−300 mM) (Supplementary Figure S11A). The protease protection presumably reflected the stabilization of the closed state of MgtE, and is consistent with the results of the patch-clamp analysis (Supplementary Figure S11B). These results indicated that these monovalent cations would not have any effect on the stabilization of the closed state of the MgtE channel at low-intracellular monovalent cation concentrations, but would exert a significant effect on the stabilization of the closed state of the MgtE channel at higher-intracellular monovalent cation concentrations (200–300 mM), which are but significantly higher than the physiological concentration.

Therefore, in the cell (under physiological conditions), Mg^{2+} is the only metal cation capable of regulating the gating of the MgtE channel. Intriguingly, these features seem to be common to both the MgtE and CorA cytosolic domains (Payandeh and Pai, 2006). Moreover, the aptamer region of the M-box riboswitch, which translationally regulates *mgtE* expression, also has this feature (Dann *et al*, 2007). Thus, the divalent-cation sensors for cellular Mg^{2+} homeostasis, regardless of whether they are formed by protein or RNA, might use common strategies against other divalent cations.

Cooperative gating control by the cytosolic domain acting as a divalent-cation sensor

Although the present analyses suggest the functional linkage between the gating event in the TM domain and the structural transition of the cytosolic domain on Mg^{2+} binding, we sought more direct functional evidence. To address this problem, we analysed the electrophysiological properties of MgtE channels with mutations at one or more of the identified divalent-cation-binding sites (Figure 2) in the cytosolic domain (D226N/D250A, E258Q, D259N, Δ1–129) (Figure 6; Supplementary Figures S12 and S13). First, all of these mutants were functionally expressed, based on the complementation of the Mg^{2+} auxotroph (Supplementary

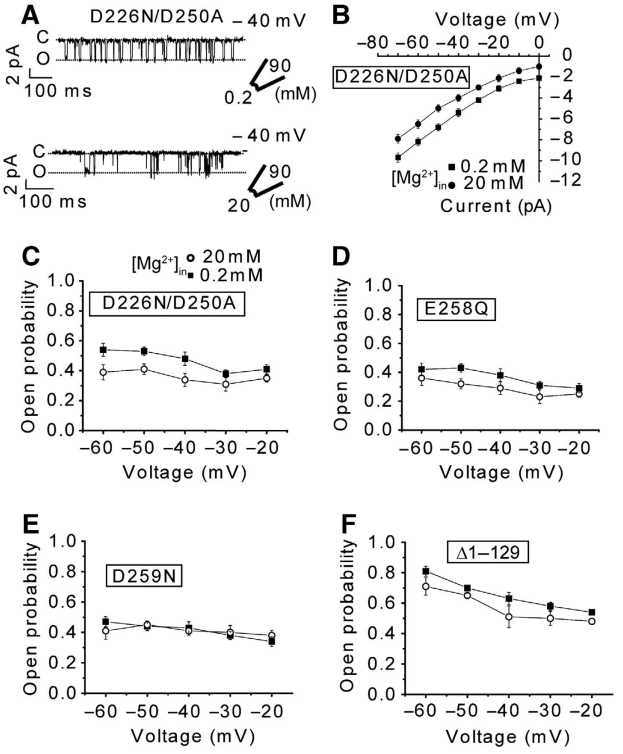

Figure 6 Gating activity of MgtE 'Mg^{2+} sensor' mutants. (**A**) Electrophysiological properties of the D226N/D250A mutant. Examples of currents recorded at −40 mV from the membrane patch of spheroplasts overexpressing the mutants at low (0.2 mM) and high (20 mM) $[Mg^{2+}]_{in}$ is shown. (**B**) The current–voltage relationships of the D226N/D250A mutant at low and high $[Mg^{2+}]_{in}$ were determined. Each experiment was repeated four times. (**C**–**F**) The open probabilities for 0.2 and 20 mM $[Mg^{2+}]_{in}$ of respective mutants ($n = 4$ for each condition).

Figure S13A). Unexpectedly, the expression of these mutants in the WT *E. coli* strain caused a dominant-negative effect on the survival of Co^{2+}-supplemented media, suggesting that the mutants exhibit Co^{2+} hypersensitivity (Supplementary Figure S13B). The Co^{2+} hypersensitivity might indirectly imply the loss of the presumed regulatory function by the MgtE cytosolic domain in these mutants, supporting our proposed MgtE-mediated Mg^{2+}-homeostasis mechanism.

To quantitatively evaluate the gating control activity, we performed patch-clamp analyses of the 'Mg^{2+} sensor' mutants. The structural transitions of the CBS domains and the adjoining plug helices from the closed to open states seem poised to directly affect the ion-transport activity, as the parallel plug helices directly occlude the cytoplasmic entrance of the ion-conducting pore in the closed state (Figure 1). Mg5 is situated at the dimer interface of the CBS domains and may neutralize the electrostatic repulsion between the acidic CBS domains, thus locking them into the closed state (Figure 2A). Mg5 is directly coordinated by the γ-carboxyl group of Asp226 and the main chain carbonyl group of Ala223 of one subunit, and through a putative water-mediated interaction with the γ-carboxyl group of Asp250 of the other subunit (Figure 2D) (Ishitani *et al*, 2008). To evaluate the effect of Mg5 on the gating control, we analysed the electrophysiological properties of the D226N/D250A double mutant. The double mutant exhibited a Mg^{2+}-dependent current, indicating that it was properly assembled in the membrane. However, the mutations largely abolished the Mg^{2+}-dependent suppression of the Mg^{2+} influx (Figure 6A). In contrast to the WT MgtE, the open probabilities of the mutant did not significantly depend on $[Mg^{2+}]_{in}$ (Figure 6C). The Mg^{2+} conductances at 0.2 and 20 mM $[Mg^{2+}]_{in}$ were almost the same for the D226N/D250A mutant (Figure 6B). The loss of the Mg5 site would probably increase the flexibility of the homodimeric MgtE cytosolic domain, thus making it more protease sensitive. Consistently, the protease protection assay revealed that the mutant was highly susceptible to proteolysis, regardless of the Mg^{2+} concentration (Supplementary Figure S14A), as compared with the Mg^{2+}-dependent protease resistance of WT MgtE (Ishitani *et al*, 2008). These data are consistent with the structural observation that the Mg5-binding site has an important function in the Mg^{2+}-dependent gating of MgtE.

Although Mg2 and 3 are situated on the plug helices, they do not bridge the two monomers (Figure 2C). Their function is apparently to neutralize the negative charges on the plug helices, thus facilitating the maintenance of the closed state. Mutations at these binding sites (E258Q for Mg2 or D259N for Mg3) also damaged the Mg^{2+}-dependent suppression of the Mg^{2+} influx (Figure 6D and E; Supplementary Figure S12), as well as the Mg^{2+}-dependent protease resistance (Supplementary Figure S14). The analysis of the open and closed dwell time histograms revealed large changes in the open dwell time of the D259N mutant (Supplementary Figure S15). These results again are consistent with our hypothesis that Mg^{2+} ions bound to the cytosolic domain stabilize the closed state of MgtE.

In contrast to the structural transition of the CBS domains, the drastic swinging away of the N domain observed in the earlier Mg^{2+}-free crystal structure (Hattori *et al*, 2007a) does not seem to be directly related to the movement of the plug helices. Therefore, despite its large movement, the function of the N domain remains elusive. However, the N domain apparently interacts with the CBS domains of the other subunit, and thus might stabilize the closed state of the cytosolic domain. Therefore, the N domain may function similar to a clamp to lock the closed state of the dimeric CBS domain (Ishitani *et al*, 2008). To test this hypothesis, we analysed the electrophysiological activities of a deletion mutant of the N domain (Δ1–129). The Δ1–129 mutation also markedly diminished the Mg^{2+}-dependent suppression of the Mg^{2+} influx (Figure 6F; Supplementary Figure S12E and F). Strikingly, the open probability of the Δ1–129 MgtE mutant was much higher than that of the WT MgtE, regardless of the intracellular Mg^{2+} concentration (Figure 6F). The analysis of the open and closed time histograms showed large changes in the open time of the Δ1–129 mutant (Supplementary Figure S15).

These results suggest that the CBS domains cannot form a stable, closed state without the N domain, and are consistent with the hypothesis that the N domain acts as a clamp to secure the CBS domains in the closed state. In this context, the Mg^{2+}-binding sites between the N and CBS domains (i.e. Mg4, 6, and 7 binding sites) may neutralize the electrostatic repulsion between the N and CBS domains to stabilize the closed state.

On the other hand, the conductances of all of the 'Mg^{2+} sensor' mutants were similar to that of the WT MgtE

(Supplementary Figure S12B). Consistent with these data, measurements of $^{57}Co^{2+}$ uptake in intact cells expressing the Δ1–129 MgtE lacking the N domain revealed almost normal uptake, with an unchanged affinity for Mg^{2+} (Supplementary Figure S16). The half-maximal inhibitory concentration ($K_{0.5}$) value, presumably corresponding to the Mg^{2+} affinity for the transmembrane domain, is below 0.1 mM (Supplementary Figure S16), which is much lower than that for the cytosolic domain (Figure 5A–F). Thus, these mutations in the cytosolic domain determine the opening and closing of the MgtE channel, but not how the pore interacts with Mg^{2+}, as the Mg^{2+} affinity for transport by these mutants did not change.

Finally, to evaluate the gating control activity of the newly identified Mg7-binding sites (Figure 2D), we performed mutational analyses of the E59A mutant (Supplementary Figure S17).

First, the E59A mutant was functionally expressed, based on the complementation of the Mg^{2+} auxotroph (Supplementary Figure S17A). The expression of the E59A mutant in the WT *E. coli* strain did not cause a dominant-negative effect on the survival in 1.125 mM Co^{2+}-supplemented media (Supplementary Figure S17B), unlike other regulatory domain mutants (Supplementary Figure S13), but it did affect the survival in 1.18 mM Co^{2+}-supplemented media (Supplementary Figure S17B). This result suggested that the E59A mutant exhibited the loss of the regulatory function to a weaker extent than those of the other regulatory domain mutants. Consistently, the E59A mutant still possessed a slight channel activity with 10 mM $[Mg^{2+}]_{in}$ (Supplementary Figure S17D), unlike the WT MgtE (Figure 5D), but not at 20 mM $[Mg^{2+}]_{in}$, unlike the other regulatory domain mutants (Figure 6). The limited proteolysis of the E59A mutant also generated a consistent result (Supplementary Figure S17F). Therefore, the Mg7-binding site would also contribute to the regulatory function of the MgtE cytosolic domain, but would have a less important function than the other cytosolic Mg^{2+}-binding sites.

Overall, the mutational analyses of the Mg2, Mg3, and Mg5-binding sites and the N domain (Mg4-, 6-, and 7-binding sites) show that the bound Mg^{2+} ions in the MgtE cytosolic domain cooperatively contribute to the formation of a stable, closed state at a high-intracellular Mg^{2+} concentration.

Discussion

In this report, the higher resolution structure of MgtE enabled us to confirm the divalent-cation binding to the MgtE cytosolic domain (Figures 1 and 2). Structure-based functional analyses revealed that MgtE is a highly Mg^{2+}-selective channel with an ion-conducting pore in the TM domain (Figures 3 and 4). Under high-intracellular Mg^{2+} conditions, the divalent-cation binding to the MgtE cytosolic domain stabilizes the closed conformation of the cytosolic domains (Supplementary Figure S14), thus inducing the stabilization of the closed state of the TM domain (Figures 5 and 6). The coupling of the conformational state between the cytosolic and TM domains would be based on the interactions between the TM domains and the plug helices (Hattori *et al*, 2007a). These X-ray crystallographic, genetic, biochemical, and electrophysiological analyses are entirely consistent. Therefore, the present channel behaviour would be related to how it functions within a cell, at least qualitatively, and partially quantitatively, although the current nature of the solution in the patch-clamp analysis differs considerably from the physiological conditions (e.g. high concentration of sucrose). These results indicate that MgtE is directly involved in cellular Mg^{2+} homeostasis. On the other hand, mammalian MgtE homologues are considered to have a different regulatory mechanism from that of bacterial MgtE, as they lack the cytosolic domain.

In contrast, under low-intracellular Mg^{2+} conditions, the MgtE channel is in equilibrium between the open and closed states in the TM domain (Figure 5A). Furthermore, the Δ1–129 mutant exhibited much higher open probability than that of the WT channel, even at low-intracellular Mg^{2+} concentrations (Figure 6F), indicating that the equilibrium of this cytosolic-domain mutant further shifts towards the channel opening state in the TM domain. Therefore, the electrophysiological property of this mutant raises the question of why the cytosolic-domain mutant affects the equilibrium in the TM domain at low-intracellular Mg^{2+} concentrations. To address this question, we made the assumption that the cytosolic domain is also in equilibrium between the open and closed states, rather than being fixed in the open state, and that the open and closed states of the cytosolic domain are coupled with the respective states in the TM domain, even at low-intracellular Mg^{2+} concentrations (Figure 7B and C). This assumption seems reasonable, as, based on the assumption, destabilization of the cytosolic domain by the Δ1–129 mutation would directly destabilize the closed state in the TM domain, resulting in the higher open probability at low-intracellular Mg^{2+} concentrations. Furthermore, this assumption is also consistent with the crystal structure, in that the interaction between the TM domains and the plug helices, which would couple the conformational states of the TM and cytosolic domains, is mainly based on the hydrophobic shape-complementarity and the dipole–dipole interactions, instead of being mediated by Mg^{2+} binding (Hattori *et al*, 2007a). We refer to this temporarily closed state as the 'transiently closed state' (Figure 7B), in which the conformations of the cytosolic and TM domains are coupled regardless of the Mg^{2+} binding to the cytosolic domain.

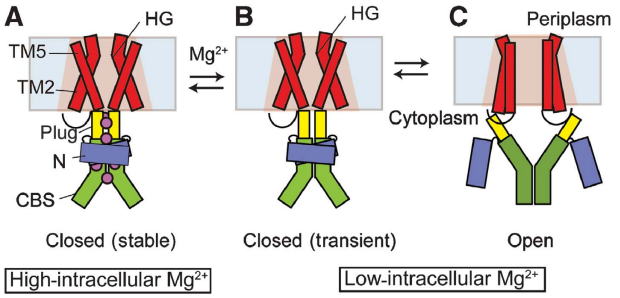

Figure 7 Proposed gating mechanism of MgtE. The colouring scheme is the same as in Figure 1. The hydrophobic gate in the MgtE pore is indicated as HG. Mg^{2+} ions are depicted as purple spheres. (**A**) The stable closed state at a high-intracellular Mg^{2+} concentration. (**B**) The transitional closed state at a low-intracellular Mg^{2+} concentration. (**C**) The open state at a low-intracellular Mg^{2+} concentration.

The three-state model shown in Figure 7 enables us to propose the transition mechanism from the open state to the stable, closed state, which is entirely consistent with our structural and functional data, and to explain how the cytosolic domain forms Mg^{2+}-binding sites, which was unclear in the earlier-proposed model. In the Mg^{2+}-bound structure, all of the Mg^{2+}-binding sites in the cytosolic domain are formed at the interfaces between the dimeric CBS domains, or the N and CBS domains, to stabilize the closed state (Figure 2). On the other hand, in the Mg^{2+}-free cytosolic-domain structure, there is no apparent Mg^{2+}-binding site, because the drastic domain rearrangement disrupts these domain interfaces (Hattori *et al*, 2007a). However, Mg^{2+}-binding sites would be temporarily formed in the transiently closed state (Figure 7B). An increase in the intracellular Mg^{2+} concentration would induce Mg^{2+} binding to either of the temporary Mg^{2+}-binding sites, which would stabilize the closed conformation of the cytosolic domain. An increase in the intracellular Mg^{2+} concentration would actually prolong the maintenance of the closed state of the channel (Figure 5A–D), based on the conformational linkage between the cytosolic and TM domains. Moreover, once Mg^{2+} binds to either of the temporary Mg^{2+}-binding sites, it would facilitate further Mg^{2+} binding to the other sites, to accomplish the formation of the stable, closed state, which is consistent with the data that the mutation of any Mg^{2+}-binding site diminished the Mg^{2+}-dependent suppression of the channel opening (Figure 6). Altogether, all of the Mg^{2+}-binding sites would cooperatively act to regulate the structural transition of MgtE in response to changes in the intracellular Mg^{2+} concentration, and thus contribute to cellular Mg^{2+} homeostasis.

Materials and methods

Crystallization

T. thermophilus MgtE (TtMgtE) was expressed and solubilized by *n*-dodecyl-β-maltoside (DDM), as described earlier (Hattori *et al*, 2007b). The solubilized supernatant was applied to an Ni–NTA (Qiagen) column equilibrated with buffer A [50 mM HEPES, pH 7.0, 150 mM NaCl], containing 0.1% (w/v) DDM and 20 mM imidazole. The column-bound proteins were washed and eluted in buffer A containing 0.25% (w/v) *n*-nonyl-β-D-thiomaltoside (NTM), and 50 and 300 mM imidazole, respectively. For further purification, the MgtE fractions were concentrated using an Amicon Ultra 30K filter (Millipore) and were applied to a HiLoad 16/60 Superdex 200 size-exclusion column (GE Healthcare), equilibrated with 20 mM HEPES (pH 7.0) buffer containing 150 mM NaCl and 0.25% (w/v) NTM. The purified protein was concentrated to approximately 10 mg/ml, using an Amicon Ultra 30K filter. The new form of the TtMgtE crystals was obtained by vapour diffusion over solutions containing 7–9% PEG 4000, 0.2 M $MgCl_2$, and 0.1 M MES, pH 6.5. Before cryo-cooling, the crystals were transferred into a cryoprotectant solution containing 9% PEG 4000, 0.2 M $MgCl_2$, 0.1 M MES, pH 6.5, and 30% PEG400. The MgtE crystals were soaked for 5–10 min in buffer B [9% (w/v) PEG4000, 0.02 M cobalt chloride, 0.15 M NaCl, 0.02 M HEPES, pH 7.0, and 0.12% (w/v) NTM] to observe the anomalous signal derived from Co^{2+}. Before cryo-cooling, the crystals were transferred into a cryoprotectant solution, composed of buffer B containing 15% PEG400 and 12% glycerol.

Data collection and structure determination

Diffraction data for full-length MgtE in the presence of Mg^{2+} were collected using an ADSC QUANTUM 315 detector on beamline BL41XU at SPring-8. Data sets of the Co^{2+}- or Ni^{2+}-soaked crystals were collected using an ADSC QUANTUM 210 detector on beamline NW12 at the Photon Factory. All diffraction data were collected at 100 K in a cold nitrogen stream and were processed with the program DENZO/SCALEPACK (Otwinowski and Minor, 1997). Phases were obtained by molecular replacement with the program MOLREP (Vagin and Teplyakov, 1997), using the earlier MgtE coordinates (PDB accession number 2YVX) as a search model. The crystallographic asymmetric unit contains one MgtE dimer. The atomic model was manually built using the program COOT (Emsley and Cowtan, 2004), and interactive cycles of refinement with PHENIX (Adams *et al*, 2002) and manual rebuilding with COOT (Emsley and Cowtan, 2004) were performed at 2.94 Å resolution. The final model contains residues 23–449 and 20–448 for chains A and B, respectively. Anomalous difference Fourier maps were generated with the CCP4 program suite (Collaborative Computational Project, No 4, 1994). Figures were produced using PYMOL (Delano, 2002). The pore in Figure 1 was calculated by the program CAVER (Petrek *et al*, 2006). A summary of the refinement statistics is provided in Supplementary Table S1.

Limited proteolysis analysis

The full-length WT and mutant MgtE proteins were prepared as described (Hattori *et al*, 2007b). The 10-μl reactions contained 8 μl of full-length MgtE (1.06 mg/ml), 1 μl of trypsin (15.6 μg/ml: Sigma), and 1 μl of 0–32 mM of divalent cation (Mg^{2+}). The reaction solutions, except for trypsin, were mixed and equilibrated at 4°C for 30–40 min. Trypsin was then added, and the reactions were incubated at 4°C for 17 h. After adding 10 μl of SDS–PAGE sample buffer, the samples were boiled and immediately subjected to 12.5% SDS–PAGE.

Gel filtration analysis

The full-length WT and D432A mutant MgtE proteins were prepared as described (Hattori *et al*, 2007b). For the gel filtration analysis in the absence of Mg^{2+}, 50 μg WT and D432A mutant MgtE proteins were applied to a Superdex 200 5/150GL size-exclusion column (GE Healthcare), pre-equilibrated with 20 mM HEPES buffer (pH 7.0) containing 150 mM NaCl and 0.05% (w/v) DDM. For the gel filtration analysis in the presence of Mg^{2+}, 50 μg WT and D432A mutant MgtE proteins in the presence of 0.2 mM $MgCl_2$ were applied to a Superdex 200 5/150GL size-exclusion column (GE Healthcare), pre-equilibrated with 20 mM HEPES (pH 7.0) buffer containing 150 mM NaCl, 0.05% (w/v) DDM, and 0.2 mM $MgCl_2$.

Strain construction and in vivo complementation assays

To construct the Mg^{2+}-auxotrophic strain with the triple endogenous gene knock-out (Δ*mgtA* Δ*corA* Δ*yhiD*; triple KO strain), which can grow only in the presence of an excess amount of Mg^{2+} (>100 mM $MgSO_4$), each gene knockout allele was constructed and transferred step-by-step to the destination strains principally by the method of Datsenko and Wanner (2000), using appropriate PCR primers (*mgtA*, *corA*) or P1 phage transduction from a systematic *E. coli* knockout library strain (*yhiD*) (Baba *et al*, 2006). For *in vivo* assays using T7 polymerase-inducible WT and mutant MgtE plasmids, lambda DE3 lysogenic strains harbouring the inducible T7 polymerase system were constructed, as described earlier (Studier *et al*, 1990). Under the non-induced conditions, that is in the absence of lactose or IPTG, these strains express a stable amount of T7 polymerase, which was sufficient for phenotypic assays in this study. The Mg^{2+}-auxotrophic strain ((BW25113) Δ*mgtA* Δ*corA* Δ*yhiD* DE3) was transformed with each plasmid, and the transformants were obtained primarily on LB (+50 μg/ml kanamycin) plates supplemented with 100 mM $MgSO_4$. Each colony was streaked on +/− Mg^{2+} plates, and colony growth was monitored by magnesium requirement-complementation assays. The WT strain (W3110 DE3) was transformed with each plasmid, and transformants were obtained primarily on LB (+50 μg/ml kanamycin) plates. Each colony was streaked on LB (+50 μg/ml kanamycin) plates supplemented with 1.125 mM $CoCl_2$ for sensitivity assays for Co^2. The expression of the *T. thermophilus* MgtE WT and mutant proteins in the membrane fraction was confirmed by anti-His tag western blotting as follows (Supplementary Figure S3A). Cultures of the *E. coli* cells (500 μl) were harvested in 200 μl of buffer A [50 mM HEPES-NaOH, pH 7.0, 150 mM NaCl, and 1 mM phenylmethylsulfonylfluoride], sonicated, and centrifuged. The supernatants were ultracentrifuged, and the pellets of the membrane fractions were resuspended in 250 μl of buffer A. The membrane fractions were mixed with sample buffer containing 4% β-mercaptoethanol, separated by 12.5% SDS–PAGE, and electrotransferred to a polyvinylidene difluoride (PVDF) membrane.

After blocking in PBS buffer containing 1% non-fat dry milk and 1% Tween-20, the PVDF membrane was incubated with an anti-His-probe (Santa Cruz Biotechnology) (1:3000), followed by an incubation in the presence of a rabbit IgG HRP (horseradish peroxidase)-linked antibody (Santa Cruz Biotechnology) (1:3000). The PVDF membrane was developed with Chemi-Lumi One (Nacalai Tesque). The signals were quantitated with an LAS-3000 imager (FUJIFILM). We used Dr Western (Oriental Yeast) as molecular markers. The expression of the *T. thermophilus* MgtE WT MgtE and mutant proteins in the membrane fraction from *E. coli* spheroplasts was similarly confirmed by anti-His tag western blotting (Supplementary Figure S3B).

Generation of spheroplasts

Giant spheroplasts, which were large enough for patch clamping, were generated by genetic and pharmacological procedures (Martinac *et al*, 1987; Kuo *et al*, 2007) (Supplementary Figure S1). To make the giant spheroplasts, cells were inoculated in 5 ml of modified LB medium (50 μl/ml kanamycin, 10 g/l tryptone, 5 g/l yeast extract, 0.5 g/l NaCl, and 100 mM $MgSO_4$) in a 14-ml test tube and were incubated aerobically by rotating at 200 r.p.m. and 37°C until the OD_{600} reached 0.3–0.5. At the desired OD_{600}, a 5-ml portion of the exponentially growing culture was diluted 10-fold into 45 ml of pre-warmed modified LB medium supplemented with 60 μg/ml cephalexin (diluted from a 6-mg/ml sterile stock solution, SIGMA #C4895) to block cell division. After 3 h of incubation by rotation at 200 r.p.m., 37°C, the un-septated filaments were harvested by centrifuging the entire culture at 3000 *g* in a 50-ml tube for 3 min. The filament pellet was then resuspended in 500 μl of 0.8 M sucrose by pipetting. A measure of 30 μl of 1 M Tris–HCl (pH 8.0), 24 μl of 0.25 mg/ml lysozyme [~10 μg/ml final concentration (~300 units), SIGMA #L6876], 6 μl of 5 mg/ml DNase I (~50 μg/ml final concentration, SIGMA #D5025), and 6 μl of 125 mM EDTA-NaOH, pH 8.0 (~1.3 mM final concentration) were sequentially added and mixed immediately in between additions by inverting the tube a few times. After an 8-min incubation at room temperature, a 100-μl aliquot of stop solution (10 mM Tris–HCl, pH 8.0, 0.7 M sucrose, 20 mM $MgCl_2$) was added to terminate the cell wall digestion. The spheroplasts were either directly used for patch clamping or frozen at −20°C.

Patch-clamp analysis

Spheroplasts (3 μl) were placed in a bath medium containing 210 mM *N*-methyl-D-glucamine, 90 mM $MgCl_2$, 300 mM D glucose, and 5 mM HEPES (pH 7.2). The spheroplasts were plated on glass coverslips 10–20 min before experiments. Borosilicate patch pipettes (Harvard Apparatus, Kent, UK), with a resistance of about 5–8 MΩ, were filled with a solution containing 210 mM *N*-methyl-D-glucamine, 90 mM $MgCl_2$ ($CaCl_2$, $MnCl_2$, $NiCl_2$, or $CoCl_2$), 300 mM sucrose, and 5 mM HEPES (pH 7.2). In some experiments, 1 mM hexammine cobalt was included in the pipette solutions. After gigal seal formation, a patch of membrane was excised and the bath solution was exchanged with a solution containing 210 mM *N*-methyl-D-glucamine, 0.2 mM $MgCl_2$, 300 mM sucrose, and 5 mM HEPES (pH 7.2). The membrane patch was voltage clamped using an Axopatch 200B amplifier (Axon CNS, Molecular Devices). The currents were filtered at 2 kHz and were sampled at 5 kHz, using a Digidata 1440A digitizer (Axon CNS).

$^{57}Co^{2+}$-transport assay

See Supplementary data.

Data deposition

The atomic coordinates have been deposited in the Protein Data Bank, www.rcsb.org (PDB ID code: 2ZY9).

Supplementary data

Supplementary data are available at *The EMBO Journal* Online (http://www.embojournal.org).

Acknowledgements

We thank the beam-line staffs at BL41XU of SPring-8 (Harima, Japan) and NW12 of KEK (Tsukuba, Japan) for technical help during data collection, Chie Tazuke for helpful discussions, and Satoshi Murakami and Yoshinori Watanabe for critical reading and improvement of this paper. This work was supported by grants from the Ministry of Education, Culture, Sports, Science and Technology (MEXT) to RI, KI, and ON, and by a grant for the National Project on Protein Structural and Functional Analyses from MEXT to ON. Additional support was provided by Promotion of Environmental Improvement for Independence of Young Researchers, Special Coordination Funds for Promoting Science and Technology from MEXT to AM, and by the Global COE Program (Center of Education and Research for Advanced Genome-Based Medicine) and Mitsubishi Foundation grants to ON.

Author Contributions: MH carried out the structure determinations, and wrote the paper, with editing from RI and ON. NI carried out the crystallization and YT assisted with it. NF performed the limited proteolysis. KI performed the *in vivo* complementation assay. AM carried out the patch-clamp analysis. MEM performed the $^{57}Co^{2+}$-transport assay. All authors discussed the results and commented on the paper. ON, KI AM supervised the work.

Conflict of interest

The authors declare that they have no conflict of interest.

References

Adams PD, Grosse-Kunstleve RW, Hung LW, Ioerger TR, McCoy AJ, Moriarty NW, Read RJ, Sacchettini JC, Sauter NK, Terwilliger TC (2002) PHENIX: building new software for automated crystallographic structure determination. *Acta Crystallogr D Biol Crystallogr* **58:** 1948–1954

Alexander RT, Hoenderop JG, Bindels RJ (2008) Molecular determinants of magnesium homeostasis: insights from human disease. *J Am Soc Nephrol* **19:** 1451–1458

Baba T, Ara T, Hasegawa M, Takai Y, Okumura Y, Baba M, Datsenko KA, Tomita M, Wanner BL, Mori H (2006) Construction of Escherichia coli K-12 in-frame, single-gene knockout mutants: the Keio collection. *Mol Syst Biol* **2:** 2006.0008

Collaborative Computational Project, No 4 (1994) The CCP4 suite: programs for protein crystallography. *Acta Crystallogr D Biol Crystallogr* **50:** 760–763

Cowan JA (2002) Structural and catalytic chemistry of magnesium-dependent enzymes. *Biometals* **15:** 225–235

Dann III CE, Wakeman CA, Sieling CL, Baker SC, Irnov I, Winkler WC (2007) Structure and mechanism of a metal-sensing regulatory RNA. *Cell* **130:** 878–892

Datsenko KA, Wanner BL (2000) One-step inactivation of chromosomal genes in Escherichia coli K-12 using PCR products. *Proc Natl Acad Sci USA* **97:** 6640–6645

Delano WL (2002) The PyMOL molecular graphics system (http: pymol.sourceforge.net/)

Emsley P, Cowtan K (2004) Coot: model-building tools for molecular graphics. *Acta Crystallogr D Biol Crystallogr* **60:** 2126–2132

Eshaghi S, Niegowski D, Kohl A, Martinez Molina D, Lesley SA, Nordlund P (2006) Crystal structure of a divalent metal ion transporter CorA at 2.9 angstrom resolution. *Science* **313:** 354–357

Goytain A, Quamme GA (2005a) Functional characterization of human SLC41A1, a Mg2 + transporter with similarity to prokaryotic MgtE Mg2 + transporters. *Physiol Genomics* **21:** 337–342

Goytain A, Quamme GA (2005b) Functional characterization of the human solute carrier, SLC41A2. *Biochem Biophys Res Commun* **330:** 701–705

Hartwig A (2001) Role of magnesium in genomic stability. *Mutat Res* **475:** 113–121

Hattori M, Tanaka Y, Fukai S, Ishitani R, Nureki O (2007a) Crystal structure of the MgtE Mg2 + transporter. *Nature* **448:** 1072–1075

Hattori M, Tanaka Y, Fukai S, Ishitani R, Nureki O (2007b) Crystallization and preliminary X-ray diffraction analysis of the full-length Mg2 + transporter MgtE. *Acta Crystallogr Sect F Struct Biol Cryst Commun* **63:** 682–684

Hmiel SP, Snavely MD, Miller CG, Maguire ME (1986) Magnesium transport in Salmonella typhimurium: characterization of magnesium influx and cloning of a transport gene. *J Bacteriol* **168:** 1444–1450

Ishitani R, Sugita Y, Dohmae N, Furuya N, Hattori M, Nureki O (2008) Mg2 + -sensing mechanism of Mg2 + transporter MgtE probed by molecular dynamics study. *Proc Natl Acad Sci USA* **105:** 15393–15398

Kehres DG, Maguire ME (2002) Structure, properties and regulation of magnesium transport proteins. *Biometals* **15:** 261–270

Kolisek M, Launay P, Beck A, Sponder G, Serafini N, Brenkus M, Froschauer EM, Martens H, Fleig A, Schweigel M (2008) SLC41A1 is a novel mammalian Mg2 + carrier. *J Biol Chem* **283:** 16235–16247

Kolisek M, Zsurka G, Samaj J, Weghuber J, Schweyen RJ, Schweigel M (2003) Mrs2p is an essential component of the major electrophoretic Mg2 + influx system in mitochondria. *EMBO J* **22:** 1235–1244

Kucharski LM, Lubbe WJ, Maguire ME (2000) Cation hexaammines are selective and potent inhibitors of the CorA magnesium transport system. *J Biol Chem* **275:** 16767–16773

Kuo A, Gulbis JM, Antcliff JF, Rahman T, Lowe ED, Zimmer J, Cuthbertson J, Ashcroft FM, Ezaki T, Doyle DA (2003) Crystal structure of the potassium channel KirBac1.1 in the closed state. *Science* **300:** 1922–1926

Kuo MM, Saimi Y, Kung C, Choe S (2007) Patch clamp and phenotypic analyses of a prokaryotic cyclic nucleotide-gated K + channel using Escherichia coli as a host. *J Biol Chem* **282:** 24294–24301

Lunin VV, Dobrovetsky E, Khutoreskaya G, Zhang R, Joachimiak A, Doyle DA, Bochkarev A, Maguire ME, Edwards AM, Koth CM (2006) Crystal structure of the CorA Mg2 + transporter. *Nature* **440:** 833–837

Martinac B, Buechner M, Delcour AH, Adler J, Kung C (1987) Pressure-sensitive ion channel in Escherichia coli. *Proc Natl Acad Sci USA* **84:** 2297–2301

Miyazawa A, Fujiyoshi Y, Unwin N (2003) Structure and gating mechanism of the acetylcholine receptor pore. *Nature* **423:** 949–955

Moomaw AS, Maguire ME (2008) The unique nature of Mg2 + channels. *Physiology (Bethesda)* **23:** 275–285

Nelson DL, Kennedy EP (1971) Magnesium transport in Escherichia coli. Inhibition by cobaltous ion. *J Biol Chem* **246:** 3042–3049

Otwinowski Z, Minor W (1997) Processing of X-ray diffraction data collected in oscillation mode. *Methods Enzymol* **276:** 307–326

Outten CE, O'Halloran TV (2001) Femtomolar sensitivity of metalloregulatory proteins controlling zinc homeostasis. *Science* **292:** 2488–2492

Payandeh J, Pai EF (2006) A structural basis for Mg2 + homeostasis and the CorA translocation cycle. *EMBO J* **25:** 3762–3773

Petrek M, Otyepka M, Banas P, Kosinova P, Koca J, Damborsky J (2006) CAVER: a new tool to explore routes from protein clefts, pockets and cavities. *BMC Bioinformatics* **7:** 316

Sahni J, Nelson B, Scharenberg AM (2007) SLC41A2 encodes a plasma-membrane Mg2 + transporter. *Biochem J* **401:** 505–513

Schindl R, Weghuber J, Romanin C, Schweyen RJ (2007) Mrs2p forms a high conductance Mg2 + selective channel in mitochondria. *Biophys J* **93:** 3872–3883

Smith RL, Thompson LJ, Maguire ME (1995) Cloning and characterization of MgtE, a putative new class of Mg2 + transporter from Bacillus firmus OF4. *J Bacteriol* **177:** 1233–1238

Splitt H, Meuser D, Borovok I, Betzler M, Schrempf H (2000) Pore mutations affecting tetrameric assembly and functioning of the potassium channel KcsA from Streptomyces lividans. *FEBS Lett* **472:** 83–87

Studier FW, Rosenberg AH, Dunn JJ, Dubendorff JW (1990) Use of T7 RNA polymerase to direct expression of cloned genes. *Methods Enzymol* **185:** 60–89

Vagin A, Teplyakov A (1997) MOLREP: an automated program for molecular replacement. *J Appl Cryst* **30:** 1022–1025

